CHEMISTRY
A EUROPEAN JOURNAL

DOI: 10.1002/chem.201103478

A Combined Solid-State NMR and X-ray Crystallography Study of the Bromide Ion Environments in Triphenylphosphonium Bromides

Kevin M. N. Burgess, Ilia Korobkov, and David L. Bryce*[a]

Abstract: Multinuclear (^{31}P and $^{79/81}$Br), multifield (9.4, 11.75, and 21.1 T) solid-state nuclear magnetic resonance experiments are performed for seven phosphonium bromides bearing the triphenylphosphonium cation, a molecular scaffold found in many applications in chemistry. This is undertaken to fully characterise their bromine electric field gradient (EFG) tensors, as well as the chemical shift (CS) tensors of both the halogen and the phosphorus nuclei, providing a rare and novel insight into the local electronic environments surrounding them. New crystal structures, obtained from single-crystal X-ray diffraction, are reported for six compounds to aid in the interpretation of the NMR data. Among them is a new structure of $BrPPh_4$, because the previously reported one was inconsistent with our magnetic resonance data, thereby demonstrating how NMR data of non-standard nuclei can correct or improve X-ray diffraction data. Our results indicate that, despite sizable quadrupolar interactions, $^{79/81}$Br magnetic resonance spectroscopy is a powerful characterisation tool that allows for the differentiation between chemically similar bromine sites, as shown through the range in the characteristic NMR parameters. $^{35/37}$Cl solid-state NMR data, obtained for an analogous phosphonium chloride sample, provide insight into the relationship between unit cell volume, nuclear quadrupolar coupling constants, and Sternheimer antishielding factors. The experimental findings are complemented by gauge-including projector-augmented wave (GIPAW) DFT calculations, which substantiate our experimentally determined strong dependence of the largest component of the bromine CS tensor, δ_{11}, on the shortest Br–P distance in the crystal structure, a finding that has possible application in the field of NMR crystallography. This trend is explained in terms of Ramsey's theory on paramagnetic shielding. Overall, this work demonstrates how careful NMR studies of underexploited exotic nuclides, such as $^{79/81}$Br, can afford insights into structure and bonding environments in the solid state.

Keywords: bromine · chemical shift tensors · NMR spectroscopy · quadrupolar interactions · solid-state structures

Introduction

Phosphonium halides are a class of compounds that contain a tetrahedral phosphorus cation with a halide counterion. They have garnered much interest in the literature because of their applications in various fields of chemistry. For instance, many of them are ionic liquids and are considered to have an advantage over the more common ammonium and imidazolium analogues, because they are less expensive and more thermally stable (i.e., higher melting points).[1] They are also usually less hygroscopic and lack an acidic proton,[2] making them ideal candidates for solvents in "green" cross-coupling reactions involving basic additives.[3] Furthermore, phosphonium halides are phase-transfer catalysts[4,5] and reagents[6,7] in the synthesis of natural products (e.g., the Wittig reaction).[8,9] Importantly, it was shown that the counterion plays a key role in the kinetics of these reactions.[10] Phosphonium halides, bearing the alkyl triphenylphosphonium (TPP) cation, have been employed as fertilisers[11] and anion receptors[12] and are known to inhibit mitochondrial function specifically in cancerous cells.[13,14,15] Recently, their role as surfactants in polymer–cellulose[16] and polymer–clay nanocomposites[17,18] has been explored. In light of the importance of this class of compounds, it is desirable to fully characterise the different components of phosphonium halides, including the local electronic environment surrounding the phosphorus and halogen nuclei, and how these relate to crystal packing. Solid-state nuclear magnetic resonance (SSNMR) is a versatile tool amenable to this type of analysis. In contrast to solution-state NMR, the different molecular orientations with respect to the static applied magnetic field, B_0, are not averaged by rapid tumbling or Brownian motion of the molecules. In a powdered sample, one obtains a SSNMR line shape that is a representation of the many different crystallite orientations present. The manifestations of this broadening are caused by perturbations of the pure Zeeman eigenstates due to the different NMR interactions. These include first the chemical shift anisotropy (CSA) that

[a] K. M. N. Burgess, Dr. I. Korobkov, Prof. D. L. Bryce
Department of Chemistry and
Centre for Catalysis Research and Innovation
University of Ottawa
10 Marie Curie Private, Ottawa, Ontario K1N6N5 (Canada)
Fax: (+1) 613-562-5170
E-mail: dbryce@uottawa.ca

Supporting information for this article is available on the WWW under http://dx.doi.org/10.1002/chem.201103478.

stems from the magnetic shielding (MS) interaction and, second, for quadrupolar nuclei (i.e., nuclear spin quantum number, I, of greater than 1/2), the usually dominating quadrupolar interaction (QI). This is defined as the coupling of the nuclear quadrupole moment and the electric field gradient (EFG) surrounding it. The interplay between these interactions depends on the electronic structure, which in turn depends upon the molecular geometry surrounding the studied nuclei, and the crystal packing in the solid state.

Herein, we report a multinuclear (i.e., ^{31}P and $^{79/81}$Br) SSNMR study of phosphonium bromides that contain the TPP moiety, with an emphasis on characterising the ^{31}P and $^{79/81}$Br chemical shift (CS) tensors. One account in the literature on the evaluation of ^{31}P CS tensor components by Ackermann et al. describes the effects of systematically replacing phenyl groups with furyl rings in ethyltriphenylphosphonium iodide.[19] They concluded that the smallest component of the CS tensor, δ_{33}, lies along the P–C(ethyl) bond, which would be consistent with Ramsey's theory of shielding (see below).[20] Since ^{79}Br and ^{81}Br are quadrupolar nuclei with $I=3/2$, additional information may be obtained by measuring the EFG tensor at the bromine nuclei. Because of the large quadrupole moments associated with bromine ($Q(^{81}\mathrm{Br})=262(3)$ mb; $Q(^{79}\mathrm{Br})=313(3)$ mb),[21] central transition (CT) line shapes are often quite broad and NMR studies in the past have been limited to relatively symmetric systems.[22,23] It is known that the broadening of the CT by the QI is inversely related to the strength of the applied magnetic field and, therefore, the design of more powerful magnets (i.e., $B_0>18.8$ T) has sparked interest in the study of these nuclei. Prior halogen NMR studies on the analogous ammonium and imidazolium halides exist.[24,25] For bromine examples, Alonso et al. reported on the study of polycrystalline $C_xH_{2x+1}(CH_3)_3NBr$ samples and have shown that variations in the value of the ^{81}Br quadrupolar coupling constant (C_Q) were owing to small changes in the N–Br distance as the alkyl chain length is increased.[26] Other noteworthy examples are those of Ripmeester and co-workers, in which they studied the halogen (^{35}Cl, ^{79}Br, and ^{127}I) counterion by solid- and liquid-state NMR in quaternary ammonium salts of ionic liquids at room temperature in an effort to observe residual order as the sample melted.[27] Bromine SSNMR experiments, performed on TPP-based phosphonium halides, will contribute to the general understanding of the relationship between the NMR parameters and the bromine local environment; in particular, we note that data on bromine CS tensors are sparse. To achieve this, single-crystal X-ray diffraction will first be employed to fully elucidate the solid-state structure of these systems.

The use of computational methods is now well established as being complementary to SSNMR measurements.[28,29] In the case of ionic solids, calculations based on cluster models are often in poor agreement with experimenal results because of the translational symmetry of the unit cell. The gauge including projector augmented wave (GIPAW) DFT method uses pseudopotentials and plane waves that are useful for describing the infinite crystal lattice and thus, more accurately describe the nature of these ionic phosphonium halides.[30,31,32,33] This method has been used by our group in the past for other systems containing bromine nuclei.[34,35] Here, the aim is that these computations will prove to be useful alongside the experimental NMR parameters when discussing the environment of the bromine nucleus in phosphonium halides.

Results and Discussion

Single-crystal X-ray diffraction studies: To relate the NMR parameters to the molecular structures of the solids studied, we first set out to acquire all the necessary X-ray crystal structures by single-crystal XRD. In this section, we report briefly on six crystal structures, that is, those of $BrEtPPh_3$, $BrMePPh_3$, $Br(C_5H_9)PPh_3$, $ClBuPPh_3$, $BrPPh_4{\cdot}H_2O$ and an updated structure for $BrPPh_4$, which was reported earlier by Schweizer et al.[36] In their structure, disorder in the bromine position was assigned to two different bromine sites in the lattice, whereas we found that the unit-cell parameters in fact match those of $BrPPh_4{\cdot}H_2O$ (see Table S3 in the Supporting Information). The results from our NMR investigations therefore prompted us to re-investigate the solid-state structure of this compound (see below). The unit-cell parameters for each of the structures are shown in Table 1. For

Table 1. Crystallographic data for new X-ray crystal structures of phosphonium halides.

	$BrEtPPh_3$	$BrMePPh_3$	$Br(C_5H_9)PPh_3$	$BrPPh_4$	$ClBuPPh_3$
crystal system	monoclinic	monoclinic	orthorhombic	triclinic	monoclinic
space group	*C*2/*c*	$P2_1/n$	*Pnma*	$P\bar{1}$	$P2_1/c$
a [Å]	14.2027(2)	9.0887(2)	15.958(2)	9.3969(8)	11.1419(3)
b [Å]	12.5625(2)	18.6129(4)	13.259(2)	10.2884(9)	9.9882(3)
c [Å]	19.7600(3)	10.5950(2)	9.2250(14)	11.2664(10)	17.2512(5)
α [°]	90.00	90.00	90.00	75.616(4)	90.00
β [°]	92.991(1)	108.030(1)	90.00	71.910(4)	103.460(1)
γ [°]	90.00	90.00	90.00	78.421(4)	90.00
V [Å^3]	3520.80(9)	1704.31(6)	1951.9(5)	993.81(15)	1867.11(9)
R_1(ref)	0.0201	0.0233	0.0214	0.0232	0.0290
wR_2(ref)	0.0558	0.0632	0.0611	0.0669	0.0866

$BrMePPh_3$, Curnow et al.[37] have reported a crystal structure that is a chloroform hemisolvate, which would not be desirable to complement our findings here because the presence of solvates in the lattice is known to alter the experimental and calculated NMR parameters.[38] As for $BrPrPPh_3$, the crystal structure, isolated as part of this study, matched with what was reported by Czerwinski.[39] The crystal structure we obtained was used for our calculations. The interpretations of the results from our crystallography studies will be discussed below in the context of the NMR parameters of the various compounds.

NMR spectroscopy

^{31}P SSNMR spectroscopy of n-alkyltriphenylphosphonium bromides: To fully characterise the phosphonium halides studied here, ^{31}P SSNMR studies were carried out, and the ^{31}P CS tensor parameters are reported in Table 2. Figure 1 shows the spectrum of a stationary sample, along with its analytical simulation and CP/MAS (cross-polarization/magic-angle spinning) spectrum for powdered $BrBuPPh_3$ at 9.4 T. ^{31}P CP/MAS and CP/static spectra were obtained for all of the other compounds considered here and are found in the Supporting Information (Figure S1). The value of δ_{iso} ranges from 21.0 to 28.1 ppm, while the value of the span ($\Omega = \delta_{11} - \delta_{33}$) varies slightly from 34 to 39 ppm. These values are consistent with those reported by Ackermann et al.[19] for the analogous ethyltriphenylphosphonium iodide, as well as those presented by Percharsky and co-workers on phosphonium salts containing the TPP moiety.[40] The CS tensor skews are all identical within experimental error. This result is not surprising because the local electronic environment about the phosphorus does not change significantly as only the length of the alkyl chain is being increased. In all five compounds discussed here, the number of phosphorus sites that is present in the MAS spectra is consistent with the solid-state structure elucidated by single-crystal XRD data.

Table 2. Experimental and calculated ^{31}P CS tensor parameters of *n*-alkyl triphenylphosphonium halides.[a]

	Exptl δ_{iso} [ppm]	Calcd δ_{iso} [ppm][b]	Exptl Ω [ppm][c]	Calcd Ω [ppm]	Exptl κ	Calcd κ
$BrBuPPh_3$	25.5(0.2)	70.9	36(1)	39.0	0.10(0.05)	−0.16
$BrPrPPh_3$	26.0(0.3)	69.1	39(2)	40.2	0.15(0.05)	0.04
$BrEtPPh_3$	28.1(0.4)	71.9	34(1)	36.6	0.20(0.05)	0.49
$BrMePPh_3$	21.0(0.5)	65.9	36(3)	39.9	0.15(0.05)	0.21
$ClBuPPh_3$	25.0(0.2)	69.4	36(2)	39.6	0.15(0.05)	−0.04

[a] Error bounds are in parentheses. [b] $\delta_{iso}(calc.) = \sigma_{iso}(H_3PO_4) - \sigma_{iso}(calc.) + \delta_{iso}(ADP) = 328.35\ ppm - \sigma_{iso}(calc.) + 0.81\ ppm$. [c] The span, $\Omega = \delta_{11} - \delta_{33}$; the skew, $\kappa = 3(\delta_{22} - \delta_{iso})/\Omega$.

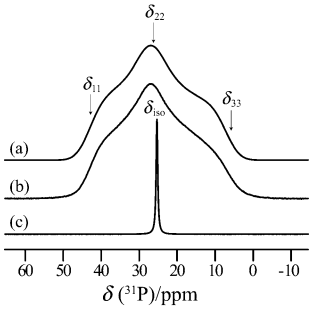

Figure 1. ^{31}P experimental CP/MAS ($\nu_{rot} = 8$ kHz; c) and CP/static (b) SSNMR spectra and simulation (a) for powdered $BrBuPPh_3$ acquired at $B_0 = 9.4$ T.

$^{79/81}$Br *SSNMR spectroscopy of triphenylphosphonium bromides*: The experimental bromine NMR parameters for each compound, considered in this work, are summarised in Table 3. These were obtained by simultaneous analytical simulations of each experimental $^{79/81}$Br NMR spectrum collected at different magnetic fields. First, ^{81}Br MAS NMR spectra were fit to extract the EFG tensor parameters (i.e., the quadrupolar coupling constant, C_Q, and the asymmetry parameter, η_Q), as well as the isotropic chemical shift, δ_{iso}, because the NMR line-shape broadening caused by CSA is eliminated under these conditions. The collection of MAS NMR spectra for all compounds was only possible at $B_0 = 21.1$ T, because the second-order quadrupolar broadening, present in powder line shapes of half-integer quadrupolar nuclei, scales inversely with B_0. After proper analysis of the MAS line shape, it was then possible to measure the remaining NMR parameters (i.e., the span, Ω, the skew, κ, and the three Euler angles, α, β, and γ, that relate the EFG and CS tensor principal axis systems (PAS)) by simulating the NMR spectra of stationary samples obtained at various values of B_0. At high magnetic fields, it is possible to extract the CSA more accurately because this effect is more pronounced and visible in the spectrum. In all cases, the ^{79}Br and ^{81}Br NMR spectra of stationary samples were collected at $B_0 = 11.75$ T (as well as $B_0 = 9.4$ T for selected cases; see Figure S2 in the Supporting Information). It is advantageous to observe both isotopes of bromine because, to a very good approximation, their NMR parameters are identical with the exception of C_Q, which scales directly by the ratio of the two quadrupole

Table 3. Experimental ^{81}Br EFG and CS tensor parameters of phosphonium bromides[a]

	$\lvert C_Q(^{81}Br)\rvert$ [b] [MHz]	η_Q	δ_{iso} [ppm]	Ω [ppm]	κ	α [°]	β [°]	γ [°]
$BrBuPPh_3$	9.48(0.10)	0.54(0.07)	130.5(5)	99(5)	0(0.05)	31(1)	72(3)	102(3)
$BrPrPPh_3$	8.48(0.20)	0.56(0.03)	121(2)	105(5)	−0.35(0.10)	43(5)	82(3)	98(2)
$BrEtPPh_3$	14.00(0.10)	0.52(0.02)	151(1)	160(10)	−0.80(0.10)	5(5)	25(2)	0(3)
$BrMePPh_3$	9.80(0.15)	0.26(0.01)	155(2)	98(3)	0.60(0.05)	59(1)	57(2)	12(10)
$Br(C_5H_9)PPh_3$	12.80(0.10)	0.62(0.01)	82(1)	140(10)	0.50(0.20)	90(5)	24(2)	90(5)
$BrHPPh_3$	14.35(0.10)	< 0.01	228(5)	305(10)	0.55(0.05)	0[c]	20(1)	90(10)
$BrPPh_4$/site A	10.50(0.05)	0.48(0.02)	3(1)	[d]	[d]	[d]	[d]	[d]
$BrPPh_4$/site B	8.55(0.05)	0.57(0.02)	46(1)	[d]	[d]	[d]	[d]	[d]

[a] Error bounds are in parentheses. Relatively small errors are the combined result of acquiring data at three fields, acquiring spectra of MAS and stationary samples, and acquiring data for both isotopes of bromine. $C_Q = eV_{33}Q/h$; $\eta_Q = (V_{11} - V_{22})/V_{33}$. [b] One typically measures the absolute value, $\lvert C_Q \rvert$. $\lvert C_Q(^{79}Br) \rvert$ is found by scaling $\lvert C_Q(^{81}Br) \rvert$ by the ratio of the quadrupole moments of both bromine isotopes (i.e., by a factor of 1.19). Both ^{79}Br and ^{81}Br experiments were performed to determine all values in this table. [c] This is inferred from the calculations and is consistent with an axially-symmetric EFG tensor. [d] It was not possible to unambiguously measure CS tensor information for this compound, owing to the presence of overlapping powder patterns for the two sites and the lack of any symmetry restrictions on the NMR parameters.

moments (for bromine, $C_Q(^{79}Br)/C_Q(^{81}Br) = Q(^{79}Br)/Q(^{81}Br) = 1.19$).[21]

The magnitude of $C_Q(^{81}Br)$ for the phosphonium halides considered here varies from 8.48 ($BrPrPPh_3$) to 14.35 MHz ($BrHPPh_3$), which is in the range of those observed for the imidazolium and ammonium solid ionic liquids studied by Ripmeester and co-workers,[27] but are on the larger end of the values reported by Alonso et al.[26] for the *n*-alkyltrimethylammonium bromides, which range from $C_Q(^{81}Br) = 6.03$ to 8.08 MHz. In terms of the isotropic chemical shifts, these are similar to those measured for the ionic liquids,[27] but varied more from compound to compound (ranging from $\delta_{iso} = 3$ to 228 ppm) than in the previous studies. As for the CS tensor span, the values obtained are larger by roughly 30 ppm compared to the ionic liquids, while the *n*-alkyltrimethylammonium bromide spans are consistent with the low end of values determined in this study. The range is from $\Omega = 98$ for $BrMePPh_3$ to 305 ppm for $BrHPPh_3$, which are comparable to the values obtained by Widdifield and Bryce for alkaline earth metal bromides.[34] Specific results and highlights are addressed below for each of the individual compounds considered in this work.

$BrMePPh_3$ crystallises in the $P2_1/n$ space group, whereas both $BrPrPPh_3$ and $BrBuPPh_3$ share a slightly different one of $P2_1/c$. The single-crystal XRD data for all three compounds show that there is one bromine site in the asymmetric unit and that it does not sit on a rotation axis or mirror plane. This indicates that neither the CS nor the EFG tensors need to have axial symmetry and no particular orientation of their PASs with respect to the molecular frame is required by the lattice symmetry. Experimental SSNMR spectra of $BrMePPh_3$ are shown in Figure 2. The value of $C_Q(^{81}Br) = (9.80 \pm 0.15)$ MHz, determined by the MAS experiment, is confirmed by simulating the stationary spectra. The CS tensor span for this sample was found to be $\Omega = (98 \pm 3)$ ppm. Observing Figure 2 more closely reveals the power and the utility of performing these experiments at many different magnetic field strengths. The splitting between the two singularities that is observed on the right-hand side of the powder pattern at $B_0 = 11.75$ T (Figure 2 h for ^{81}Br) increases at $B_0 = 21.1$ T (Figure 2 d). Furthermore, this splitting is greatly reduced for the stationary ^{79}Br NMR spectrum at $B_0 = 11.75$ T (Figure 2 f). These distinct spectral features are attributed to the more important role of CSA in the higher magnetic field. The same observations can be made for $BrPrPPh_3$ (Figure 3), where the span of (105 ± 5) ppm is close to that of $BrMePPh_3$. However, the values of $C_Q(^{81}Br)$ determined for the two samples differ by approximately 1 MHz. For $BrBuPPh_3$ (Figure 4), the experimentally extracted Euler angles are close to the values for $BrPrPPh_3$ and, as is the case with all of the *n*-alkyl TPP bromides, the asymmetry parameters of both the CS and the EFG tensors are representative of a bromine ion not positioned on any particular symmetry axis or plane, which is consistent with the reported X-ray crystal structures. As for the value of $\Omega = (99 \pm 5)$ ppm, this is very close to the values for the propyl and methyl analogues.

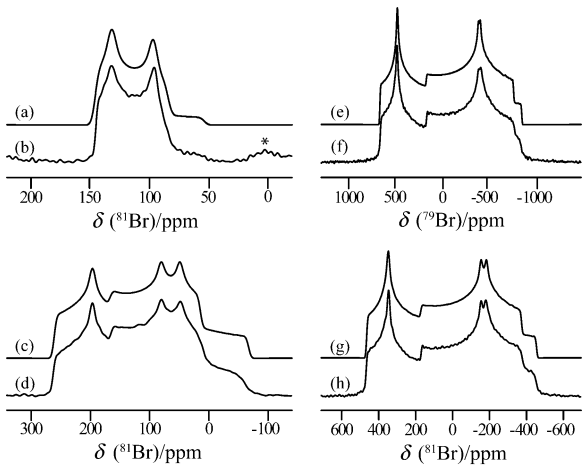

Figure 2. $^{79/81}Br$ solid-state NMR spectra of powdered $BrMePPh_3$. An experimental ^{81}Br MAS NMR spectrum ($\nu_{rot} = 31.25$ kHz; b) was acquired at $B_0 = 21.1$ T (the visible spinning sideband is marked *). A ^{79}Br NMR spectrum was acquired at $B_0 = 11.75$ T (f) and ^{81}Br NMR spectra were acquired at $B_0 = 21.1$ (d) and 11.75 T (h), all under stationary conditions. All analytical simulations (a, c, e, and g) were performed by using WSolids (data in Table 3). Complementary $^{79/81}Br$ NMR data at $B_0 = 9.4$ T, along with their analytical simulations, can be found in Figure S2 of the Supporting Information.

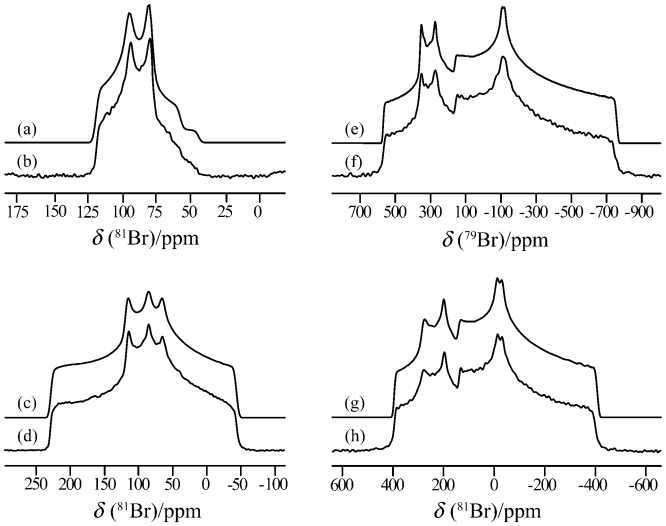

Figure 3. $^{79/81}Br$ solid-state NMR spectra of powdered $BrPrPPh_3$. An experimental ^{81}Br MAS NMR spectrum ($\nu_{rot} = 31.25$ kHz; b) was acquired at $B_0 = 21.1$ T. A ^{79}Br NMR spectrum was acquired at $B_0 = 11.75$ T (f) and ^{81}Br NMR spectra were acquired at $B_0 = 21.1$ (d) and 11.75 T (h), all under stationary conditions. All analytical simulations (a, c, e, and g) were performed by using WSolids (data in Table 3). Complementary $^{79/81}Br$ NMR data at $B_0 = 9.4$ T, along with their analytical simulations, can be found in Figure S2 of the Supporting Information.

Recently, Wu and Terskikh[41] have shown that C_Q is related linearly to the quantity $Q(1-\gamma_\infty)/V$, in which γ_∞ is the Sternheimer antishielding factor that is unique to each atomic type and where V is the unit cell volume from XRD experiments, for a series of isostructural compounds. This

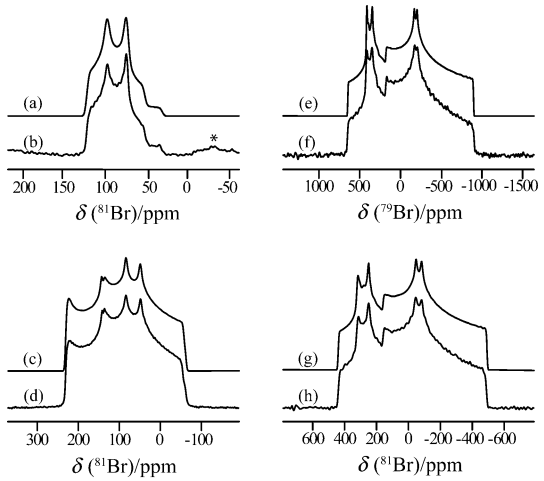

Figure 4. $^{79/81}$Br solid-state NMR spectra of powdered $BrBuPPh_3$. An experimental ^{81}Br MAS NMR spectrum ($\nu_{rot}=31.25$ kHz; b) was acquired at $B_0=21.1$ T (the visible spinning sideband is marked with *). A ^{79}Br NMR spectrum was acquired at $B_0=11.75$ T (f) and ^{81}Br NMR spectra were acquired at $B_0=21.1$ (d) and 11.75 T (h), all under stationary conditions. All analytical simulations (a, c, e, and g) were performed using WSolids (data in Table 3). Complementary $^{79/81}$Br NMR data at $B_0=9.4$ T, along with their analytical simulations, can be found in Figure S2 of the Supporting Information.

type of relationship has also been discussed and demonstrated for many Group 2 metal halides and their hydrates,[34,38,42] and we attempt here to further extend this trend to halogen nuclei in phosphonium halides. This knowledge would be useful to estimate and confirm experimental C_Q values within a series of analogous compounds, which finds applicability in the field of NMR crystallography. $BrBuPPh_3$ and $ClBuPPh_3$ should be nominally isostructural ($P2_1/c$ space group), which suggests that the $C_Q(^{81}Br)/C_Q(^{35}Cl)$ and $[Q_{^{81}Br}(1-\gamma_{\infty(^{81}Br)})/V]/[Q_{^{35}Cl}(1-\gamma_{\infty(^{35}Cl)})/V]$ ratios should be close. To accurately determine the value of $C_Q(^{35}Cl)$ for $ClBuPPh_3$, SSNMR experiments under MAS conditions were performed at $B_0=9.4$ T (Figures 5d and f for ^{35}Cl and ^{37}Cl, respectively) and at $B_0=21.1$ T (Figure 5b). The experimental value of $C_Q(^{35}Cl)$ is (1.13 ± 0.01) MHz, whereas the value of $C_Q(^{37}Cl)=(0.88\pm0.01)$ MHz is in perfect agreement with the value expected by evaluating the product between the ratio of both quadrupole moments (i.e., $Q(^{37}Cl)/Q(^{35}Cl)$) and the value of $C_Q(^{35}Cl)$. Using the experimental SSNMR

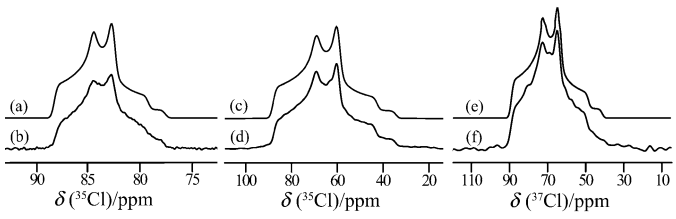

Figure 5. $^{35/37}$Cl solid-state NMR spectra of powdered $ClBuPPh_3$. Experimental MAS NMR spectra were acquired for ^{35}Cl at $B_0=21.1$ (b) and 9.4 T (d) and for ^{37}Cl at $B_0=9.4$ T (f). Analytical simulations (a, c, and e) resulted in the following NMR parameters: $C_Q(^{35}Cl)=(1.13\pm0.01)$ MHz, $C_Q(^{37}Cl)=(0.88\pm0.01)$ MHz, $\eta_Q=(0.65\pm0.01)$ and $\delta_{iso}=(88.5\pm0.5)$ ppm.

data, the value of $C_Q(^{81}Br)/C_Q(^{35}Cl)$ is 8.39. From the crystallographic data, the ratio $[Q_{^{81}Br}(1-\gamma_{\infty(^{81}Br)})/V]/[Q_{^{35}Cl}(1-\gamma_{\infty(^{35}Cl)})/V]$ is calculated to be 6.11, a 37% difference, consistent with previous studies on the Group 2 metal chlorides and bromides.[34,38] A key contribution to this error lies in the fact that $ClBuPPh_3$ and $BrBuPPh_3$ are not precisely isostructural, even if they belong to the same space group. The position of the halide ion in each crystal structure is slightly different; for $BrBuPPh_3$, $x/a=0.37978(2)$, $y/b=0.1368(3)$, $z/c=0.83347(1)$[55] and for $ClBuPPh_3$, $x/a=0.37565(3)$, $y/b=0.12066(3)$, $z/c=0.83537(2)$. We note here that the most significant change in the anion position is with respect to y/b and that this is a similar difference as what was observed for the $CaBr_2/CaCl_2$ pair.[38] It has been shown in previous studies that changing the bromide position by a very small increment (<0.05 Å) can substantially affect the value of $C_Q(^{81}Br)$.[35]

The final compound studied in the *n*-alkyl TPP bromide family, $BrEtPPh_3$, had some of the broadest line shapes in this study, which can be found in Figure 6. In contrast to the

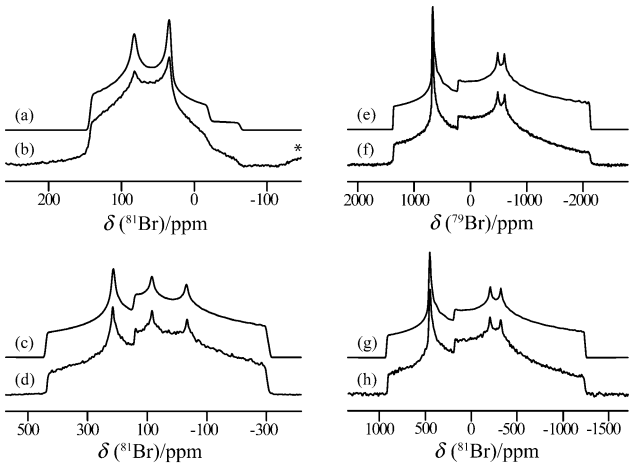

Figure 6. $^{79/81}$Br solid-state NMR spectra of powdered $BrEtPPh_3$. An experimental ^{81}Br MAS NMR spectrum ($\nu_{rot}=62.5$ kHz; b) was acquired at $B_0=21.1$ T (the visible spinning sideband is marked with *). A ^{79}Br NMR spectrum was acquired at $B_0=11.75$ T (f) and ^{81}Br NMR spectra were acquired at $B_0=21.1$ (d) and 11.75 T (h), all under stationary conditions. All analytical simulations (a, c, e, and g) were performed using WSolids (data in Table 3). Complementary $^{79/81}$Br NMR data at $B_0=9.4$ T, along with their analytical simulations, can be found in Figure S2 of the Supporting Information.

methyl, propyl, and butyl adducts, $BrEtPPh_3$ is characterised by a notably larger $C_Q(^{81}Br)$ value of (14.00 ± 0.10) MHz. This type of observation can also be made for the value of Ω, which is on average 100 ppm for the other *n*-alkyl TPP bromides and 160 ppm for $BrEtPPh_3$. This suggests that $BrEtPPh_3$ does not crystallise in the same fashion as the analogous compounds. These NMR data prompted us to seek independent confirmation by X-ray diffraction, which indeed showed that $BrEtPPh_3$ crystallises in the $C2/c$ space group, thereby demonstrating the power of SSNMR in detecting small structural changes among a set of chemically similar compounds.

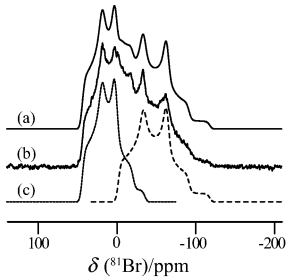

Figure 7. Experimental ^{81}Br MAS NMR spectrum of powdered $BrPPh_4$, $\nu_{rot}=62.5$ kHz (b), acquired at $B_0=21.1$ T. The analytical simulation (a) required two bromine sites to properly fit the spectrum with the parameters shown in Table 3. The deconvolution of this simulation is shown in (c).

Shown in Figure 7 is the ^{81}Br MAS NMR spectrum acquired at $B_0=21.1$ T, along with analytical simulations (including a deconvolution of the individual line shapes) associated with what is clearly two distinct bromine sites for $BrPPh_4$. Spectra of the stationary sample (not shown) have been acquired at multiple fields, but a unique and accurate analytical simulation, including all of the CSA and EFG tensor parameters and their relative orientations for the two sites, proved to be quite difficult, owing to the large number of adjustable parameters. As shown in Figure 7c, both powder patterns exhibit similar quadrupolar asymmetry parameters η_Q, (0.48 ± 0.02) and (0.57 ± 0.02) for sites A and B, respectively. The major differences lie in the values of $\delta_{iso}=(3\pm1)$ and (46 ± 1) ppm for sites A and B, as well as the width of the two powder patterns, which are directly related to the quadrupolar coupling constants. The most shielded resonance (site A) is broader and characterised by a $C_Q(^{81}Br)$ of (10.50 ± 0.05) MHz, whereas the narrower site B has a smaller $C_Q(^{81}Br)$ of (8.55 ± 0.05) MHz. The previously reported crystal structure by Schweizer et al.[36] is not consistent with the aforementioned results, since the NMR line shape does not exhibit any form of disorder or fractional occupancy, as would be expected from its proposed structure. Our revised crystal structure packs in the $P\bar{1}$ space group and now has two crystallographically distinct bromine sites (each with 100% occupancy) that both sit on inversion centres, which is in full agreement with our NMR experiments. We are confident that our structure is an improvement over the latter because we obtained an R_1 of 2.32% compared to 5.75% obtained previously (see Table 1). This result further demonstrates how SSNMR spectra can corroborate or refute X-ray crystallographic data and that SSNMR can distinguish between what are seemingly chemically identical bromine sites in organic materials.

$Br(C_5H_9)PPh_3$ (Figure 8) and $BrHPPh_3$ (Figure 9) both crystallise in the *Pnma* space group and each has a single bromine site that sits on a mirror plane. This dictates that one of the principal components of the EFG tensor and another from the CS tensor must be collinear and perpendicular to the plane. For $Br(C_5H_9)PPh_3$, the experimental Euler angles ($\alpha=90$, $\beta=24$, and $\gamma=90°$) indicate geometrically

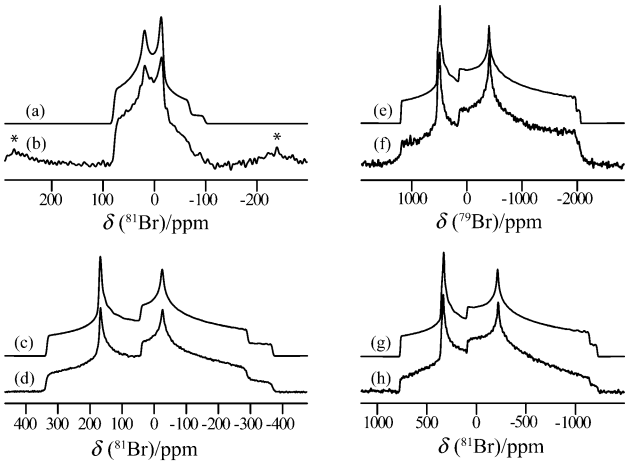

Figure 8. $^{79/81}$Br solid-state NMR spectra of powdered $Br(C_5H_9)PPh_3$. An experimental ^{81}Br MAS NMR spectrum ($\nu_{rot}=62.5$ kHz; b) was acquired at $B_0=21.1$ T (the visible spinning sidebands are marked with *). A ^{79}Br NMR spectrum was acquired at $B_0=11.75$ T (f) and ^{81}Br NMR spectra were acquired at $B_0=21.1$ (d) and 11.75 T (h), all under stationary conditions. All analytical simulations (a, c, e, and g) were performed using WSolids (data in Table 3).

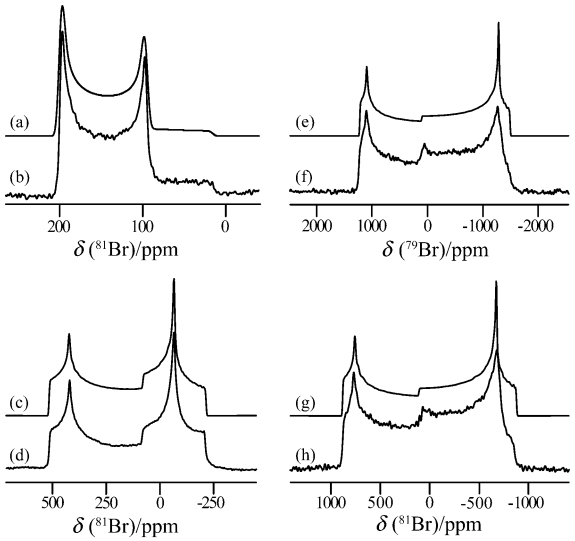

Figure 9. $^{79/81}$Br solid-state NMR spectra of powdered $BrHPPh_3$. An experimental ^{81}Br MAS NMR spectrum ($\nu_{rot}=62.5$ kHz; b) was acquired at $B_0=21.1$ T (the spinning sidebands were added into the centre band to ensure a more accurate simulation). A ^{79}Br NMR spectrum was acquired at $B_0=11.75$ T (f) and ^{81}Br NMR spectra were acquired at $B_0=21.1$ (d) and 11.75 T (h), all under stationary conditions. All analytical simulations (a, c, e, and g) were performed using WSolids (data in Table 3).

that both the smallest component of the EFG tensor, V_{11}, and the largest component of the CS tensor, δ_{11}, are coincident, whereas in the case of $BrHPPh_3$, V_{22} and δ_{11} are collinear. It is clear from the ^{81}Br MAS spectrum at $B_0=21.1$ T for $BrHPPh_3$ (Figure 9b) that the EFG tensor is axially symmetric (i.e., $\eta_Q<0.01$), in contrast to that observed for $Br(C_5H_9)PPh_3$ where $\eta_Q=(0.62\pm0.01)$, a value similar to those of the *n*-alkyl TPP bromides (see Table 3). Although both compounds share identical space groups, $BrHPPh_3$ has the

largest $C_Q(^{81}Br)$ of the compounds characterised by SSNMR in this study, (14.35 ± 0.10) MHz, as well as the largest CS tensor span of $\Omega = (305 \pm 10)$ ppm and isotropic chemical shift of $\delta_{iso} = (228 \pm 5)$ ppm.

We next sought to address the origins of the large range in the values of Ω (98 to 305 ppm) that characterises the TPP bromides studied, which was not observed in the studies on long-chain *n*-alkyltrimethylammonium bromides, for which the span ranged between $\Omega = 105$ and 117 ppm (standard deviation of 6 ppm).[26] We found that in all the TPP bromides studied here, the bromine CS tensor span for a given compound correlates with the shortest bromine–phosphorus distance measured by single-crystal XRD. The correlation is such that larger spans are observed when this distance is shorter (Figure 10a). Since this parameter is representative of the difference between the largest and the smallest components of the CS tensor (i.e., $\Omega \approx \delta_{11} - \delta_{33}$), there should be a correlation between either δ_{11} or δ_{33} and the Br–P distance. A better correlation between δ_{11} and the shortest Br–P distance is noted (Figure 10b), as quantified by the R value which changes from 0.950 (for Ω) to 0.973 (for δ_{11}). This type of observation demonstrates how one can relate the crystal structure of a compound to the NMR parameters, as distinct structural differences manifest themselves in the NMR spectrum, which has applicability in NMR crystallography. The use of computational methods are therefore expected to greatly aid in determining the reasons behind this experimentally observed trend. Likewise, computations make it possible to assign the EFG and CS tensor orientations in the molecular frame.

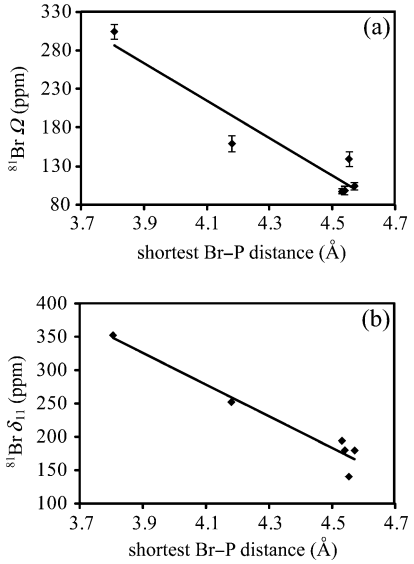

Figure 10. Plots of the experimental CS tensor parameters Ω (a) and δ_{11} (b) as a function of the shortest Br–P (d_{Br-P}) distance in the crystal structures of compounds studied. The lines of best fit are as follows: (a) $\Omega(^{81}Br, \text{expt.}) = -242.81(d_{Br-P}) + 1210.6$, $R = 0.950$; (b) $\delta_{11}(^{81}Br, \text{expt.}) = -237.55(d_{Br-P}) + 1253$, $R = 0.973$.

GIPAW DFT calculations: We briefly comment on the GIPAW DFT-calculated ^{31}P MS tensor parameters for the *n*-alkyl TPP halide compounds. First of all, the magnitudes of the span are very well predicted, as is evidenced in Table 2 for all samples considered. For the skew, the agreement is quite good with the exception of $BrEtPPh_3$, whereas the isotropic chemical shift is overestimated in all cases by approximately 40 ppm when using the absolute shielding scale for ^{31}P. GIPAW DFT calculations have previously been performed on the ^{31}P nucleus in aluminophosphates by Ashbrook et al.[43] Their values, however, were not interpreted in terms of an absolute shielding scale, but rather with respect to an optimal experimentally determined value within their studied systems. Using this method, they obtained poor agreement between the relative experimental and calculated isotropic chemical shifts. In contrast to their study, the relative chemical shifts computed here for the phosphonium halides agree fairly well with the experimental shifts. For example, the lowest experimental δ_{iso} ((21.0 ± 0.5) ppm for $BrMePPh_3$) has the lowest calculated shift of $\delta_{iso} = 65.9$ ppm, while the highest experimental δ_{iso} ((28.1 ± 0.4) ppm for $BrEtPPh_3$) has the highest calculated isotropic chemical shift of $\delta_{iso} = 71.9$ ppm. We investigated whether the overestimation in the ^{31}P chemical shifts could stem in part from spin-orbit relativistic effects, associated with the nearby bromide ion.[44,45] Amsterdam Density Functional (ADF) calculations under the zeroth-order regular approximation (ZORA) were performed to address this hypothesis because spin-orbit and scalar relativistic effects can be considered. The calculated ^{31}P isotropic shielding for a crude model of $BrBuPPh_3$ increases by about 9 ppm (3%) when compared to a calculation without considering relativistic effects (see Table S4 in the Supporting Information).

The GIPAW DFT calculations also provide insight into the orientations of the MS eigenvectors with respect to the molecular frame. It was found that σ_{33} is oriented approximately 35° away from the P–CH_2 bond in all of the *n*-alkyl TPP halides. In $BrBuPPh_3$ this angle is 36.0° and in $ClBuPPh_3$ it is 37.4° (see Figure S3 in the Supporting Information). This is consistent with the conclusions reached by Ackermann et al. for ethyltriphenylphosphonium iodide, where the angle between σ_{33} and the P–C(ethyl) bond vector was 39.3° (calculated with the B3LYP hybrid DFT functional).[19] Although a relatively good agreement (root mean square deviation (rmsd) of 4.2 ppm) between the experimental and calculated magnitudes of Ω and δ_{iso} was obtained when using the phosphoric acid absolute shielding scale, their models did not include the halide anions, whereas these are included in our GIPAW DFT calculations. Therefore, we performed these calculations on our structures, while excluding the halogen ions and accounting for the resulting charge of the unit cell. Although the value of the span was still well predicted, we observed a change in the orientation of the σ_{33} eigenvector with respect to the P–CH_2 bond vector. In the case of $BrBuPPh_3$ and $ClBuPPh_3$, this angle changed to 48.7° and 48.5°, respectively (see Figure S3 in the Supporting Information). This is in disagree-

ment with the models used by Ackermann et al. and suggests that it is important to always include the halide anion in the calculation of these ^{31}P MS tensors when performing GIPAW DFT calculations on these systems. We note in passing that B3LYP calculations using a cluster model were attempted on the phosphonium bromides and these did not yield results consistent with the those of Ackerman et al.

In Table 4 the GIPAW DFT-calculated ^{81}Br EFG and CS tensor parameters for the phosphonium halides are shown. It is evident that $C_Q(^{81}Br)$ is well predicted with an rmsd of

Table 4. Calculated $^{79/81}Br$ EFG and CS tensor parameters for phosphonium bromides using GIPAW DFT.

	$C_Q(^{81}Br)$ [MHz]	η_Q	δ_{iso} [ppm]	Ω [ppm]	κ	α [°]	β [°]	γ [°]
$BrBuPPh_3$	−9.35	0.79	54.6	151	0.06	47	89	68
$BrPrPPh_3$	−8.98	0.59	25.4	162	−0.01	61	71	116
$BrEtPPh_3$	−10.78	0.84	87.9	292	−0.78	74	89	52
$BrMePPh_3$	6.74	0.34	47.3	156	−0.53	65	44	140
$Br(C_5H_9)PPh_3$	−65.52	0.24	3.4	314	−0.42	90	15	90
$BrHPPh_3$	−74.85	0.00	359.8	726	0.85	0	9	90
$BrPPh_4$/site 1	13.20	0.28	−88.3	257	0.19	45	74	123
$BrPPh_4$/site 2	12.50	0.34	16.0	365	0.32	67	77	4

2.24 MHz (up to 31% error for $BrMePPh_3$ and as low as 1% for $BrBuPPh_3$) for the *n*-alkyl TPP bromides, whereas for $Br(C_5H_9)PPh_3$ and $BrHPPh_3$ this is not the case. It has been shown before that in this type of calculation, any inaccuracy in the position of the halogen or the surrounding atoms may result in very large errors in the predicted $C_Q(^{81}Br)$.[35] As the solid-state structures input into the calculations were generated from X-ray diffraction data, the positions of the hydrogen atoms are not known exactly and thus, their positional optimisation is desirable. Unfortunately, since the unit cell volumes of the structures considered here were too large (i.e., $V > 1500$ Å^3), it was not computationally feasible with our infrastructure, as was the case with some of the amino acid hydrochlorides reported by Chapman et al.[46] If one compares the crystal structure of $BrBuPPh_3$ (for which the calculated $C_Q(^{81}Br)$ is predicted within 1% of the experimental value) with that of $BrHPPh_3$ (for which this is 5 times greater than the experimental value determined by MAS), it can be shown that the closest hydrogen atom in the lattice is much closer to the bromide anion (2.25 Å) than in $BrBuPPh_3$ (2.84 Å). Granted in $Br(C_5H_9)PPh_3$, the closest hydrogen atom is at an unoptimised position of 2.54 Å (i.e., farther than in $BrHPPh_3$), but a wagging disorder in the cyclopentyl ring adjacent to the bromine atom may contribute to the large inaccuracy of its predicted $C_Q(^{81}Br)$. These effects on the value of $C_Q(^{81}Br)$, owing to the proximity of the closest hydrogen atoms, have been observed before in the case of glycyl-L-alanine $HBr{\cdot}H_2O$, in which V_{33} for bromine was oriented towards the nearest hydrogen atom.[47] As for $BrPPh_4$, the two different crystallographic sites yield different calculated values for their $C_Q(^{81}Br)$, which was observed experimentally. The ratio of $C_Q(^{81}Br)_{site1}/C_Q(^{81}Br)_{site2}$ of 1.06 is close to the observed ratio of 1.23 for $C_Q(^{81}Br)_{siteA}/C_Q(^{81}Br)_{siteB}$, which corresponds to a difference of nearly 14%. When visualising the EFG tensor eigenvectors with respect to the molecular frame, V_{33} is oriented towards the closest parallelepiped formed by the nearest TPP cation, which is consistent with computations made by Alonso et al. in their study of the analogous *n*-alkyltrimethylammonium bromide salts with B3LYP calculations.[26]

Shown in Figure 11b is a plot of the GIPAW DFT-calculated versus the experimental values of δ_{iso}. The computed isotropic chemical shift is significantly overestimated in the

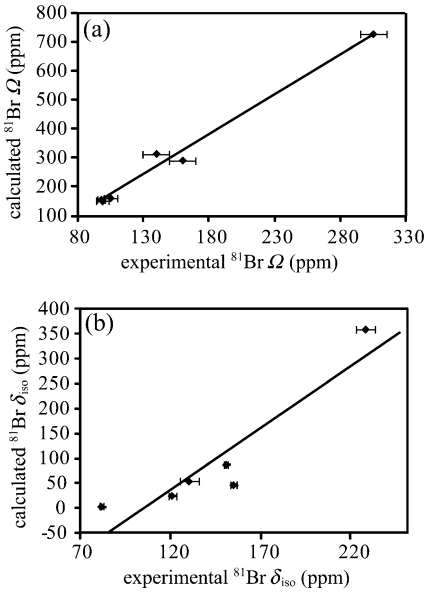

Figure 11. The GIPAW DFT calculated Ω (a) and δ_{iso} (b) plotted versus their experimental values for TPP bromides. The lines of best fit are as follows: (a) $\Omega(^{81}Br, calc.) = 2.763(\Omega(^{81}Br, expt.)) - 117.36$, $R = 0.993$; (b) $\delta_{iso}(^{81}Br, calc.) = 2.502(\delta_{iso}(^{81}Br, expt.)) - 265.2$, $R = 0.919$.

calculations by approximately the same amount in all of the compounds studied; thus, there is a good overall correlation (Pearson's correlation coefficient $R = 0.919$). In the case of $BrPPh_4$, these calculations permit us to tentatively assign each bromine site in the crystal structure of that compound. Site A has a slightly higher experimental $C_Q(^{81}Br)$, but a smaller η_Q and δ_{iso}, which is consistent with site 1 in the calculations. This site corresponds to the bromide ion lying further from the phosphorus cation ($d_{Br-P} = 6.24$ Å). Site 2, which corresponds to the shortest Br–P distance (5.50 Å), is therefore assigned to site B.

Like the δ_{iso} values, it is observed that the calculated spans are overestimated compared with the experimental values. When converting our experimental results from Table 3 to their individual components in the CS tensor PAS (i.e., δ_{11}, δ_{22}, and δ_{33}) and comparing them to the calculated parameters, we see an overestimation of δ_{11} by an amount similar to that of Ω, whereas δ_{33} is more accurately predicted. We speculate that this systematic overestimation could stem from relativistic effects and/or our inability to optimise

the hydrogen positions in our structures. ADF calculations (see these results in Table S4 of the Supporting Information) show that including relativistic effects under ZORA does not change Ω significantly. Once hydrogen positions are optimised on a crude model system (with the Gaussian '09 software), the increase in σ_{11} is sixfold that of σ_{33}, suggesting that the former is much more susceptible to this action. We wish to emphasise here that the ADF calculations are cluster-model-based and that GIPAW DFT still more accurately predicts the span. Because of the strong correlation between the Ω values calculated by GIPAW DFT and the experimentally determined values (R value of 0.993, see Figure 11 a), along with their small error margins, we sought to investigate the experimental correlation between δ_{11} and the smallest Br–P distance in the crystal structure. Figure 12 a shows that the experimental trend is corroborated by GIPAW DFT calculations, where the largest component of the calculated CS tensor in its PAS is inversely related to the shortest Br–P distance (R value of 0.969).

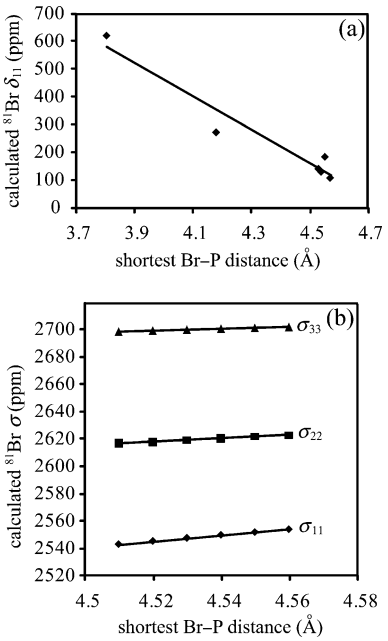

Figure 12. The GIPAW DFT calculated δ_{11} for all phosphonium halides (a) and σ_{ii} ($i=1, 2, 3$) of $BrBuPPh_3$ (b) as a function of the shortest Br–P distance present in the crystal structure. The lines of best fit are as follows: (a) $\delta_{11}(^{81}Br, calc.) = -606.04(\delta_{11}(^{81}Br, expt.)) + 2885.9$, $R = 0.969$; (b) $\sigma_{11}(^{81}Br, calc.) = 220.6(d_{Br-P}) + 1548$, $R = 1.000$ and $\sigma_{22}(^{81}Br, calc.) = 122.6(d_{Br-P}) + 2064$, $R = 0.999$ and $\sigma_{33}(^{81}Br, calc.) = 63.3(d_{Br-P}) + 2413$, $R = 0.998$.

When visualising the calculated orientations of the different eigenvectors of the MS tensor PAS in the molecular frame, it is evident that, in all cases, σ_{11} is oriented approximately 90° from the internuclear vector that corresponds to the shortest Br–P distance in the crystal structure (see Figure S4 in the Supporting Information). This result may be interpreted by considering the effects of paramagnetic shielding on the bromine nucleus. According to Ramsey,[20] MS may be described by using diamagnetic and paramagnetic terms (i.e., $\sigma = \sigma_{dia} + \sigma_{para}$), in which the latter is an indication of the degree of mixing between occupied and virtual wave functions which contribute to a particular shielding component. To probe the effects on the individual components of the MS tensor when the Br–P distance is systematically changed in the crystal structure, we performed multiple GIPAW DFT calculations on $BrBuPPh_3$, in which the bromine atom is displaced along the direction of the Br–P internuclear vector. It is clear from Figure 12 b that the most sensitive MS tensor component to this action is σ_{11} because the slope of this curve is 221 versus 123 ppm Å^{-1} for σ_{22} and 63 ppm Å^{-1} for σ_{33}. This is consistent with Ramsey's theory, which, in this case, makes σ_{11} (or δ_{11}) the axis of rotation about which one of the bromide ion's p-type molecular orbitals (MO) will rotate 90° to favourably overlap with a virtual one, resulting in a paramagnetic contribution to shielding. In fact, a decrease in the Br–P distance results in a decrease of $\sigma_{11,para}$ and because this term is negative, this results in an overall smaller σ_{11}. A smaller value of σ_{11} corresponds to a larger δ_{11}, which is consistent with the experimentally observed trend shown in Figure 10. We additionally performed ADF calculations with the revPBE functional and the TZ2P basis set on all atoms to validate our hypothesis. Although this method is again cluster-model-based, these computations allow one to relate molecular orbitals to the diamagnetic and paramagnetic contributions to the overall shielding of the nucleus. Here, we used a model of $BrBuPPh_3$ and displaced the bromine nucleus along the Br–P internuclear vector. The results indicate an occupied MO with p character centred on Br^- that, when rotated 90° about the direction of σ_{11}, overlaps with a similar virtual orbital, thereby generating a paramagnetic contribution to shielding, which changes most significantly upon varying the Br–P distance, which is in full agreement with Ramsey's theory.

Conclusion

In summary, solid-state NMR techniques, including challenging $^{79/81}$Br experiments, have been employed with a range of applied magnetic field strengths, and the $^{79/81}$Br EFG and CS tensors for six TPP-cation-bearing phosphonium bromides of broad interest and application have been characterised. To relate these parameters to the molecular and crystal structures of these compounds, six new crystal structures were solved by single-crystal XRD, including an updated structure for $BrPPh_4$ because the experimental SSNMR data extracted for this particular compound were not consistent with the reported crystal structure in the literature. It was found that small structural changes, which include the presence or absence of site symmetry elements, between each compound can manifest themselves in the NMR parameters, as seen in the large ranges (hundreds of ppm) in the bromine CS tensor span and in the isotropic chemical shifts. These findings are non-trivial for nuclides in

which large quadrupolar interactions typically dominate the NMR spectra, such as $^{79/81}$Br, and demonstrate the power of SSNMR of nuclei that are typically thought of as difficult in detecting changes in crystal packing between nearly identical compounds.

Valuable information was also extracted from the results of GIPAW DFT calculations, which employed the crystal-structure data of the studied compounds. These have an advantage over cluster-based calculations, because they account for the periodicity of the structure and thus, are well suited for predicting the NMR parameters of the ionic phosphonium halides. For the calculation of ^{31}P shielding tensors, the span was well predicted within experimental error, while the isotropic chemical shift was systematically overestimated using the ^{31}P absolute shielding scale. In addition, it was deemed important to include the halide ion in the calculations, as its exclusion resulted in errors in the CS tensor's orientation with respect to the molecular frame. It was possible to relate important structural features of the molecules and their crystal structures to the NMR parameters. For instance, the calculations substantiate the experimentally determined strong dependence of the largest component of the bromine CS tensor, δ_{11}, on the shortest Br–P distance in the crystal structure, an exciting finding which shows that CS tensors (not just quadrupolar interactions) for exotic nuclei, such as $^{79/81}$Br, can be used to provide insight into the structure and therefore has possible application in the field of NMR crystallography. These calculations also permitted us to distinguish between the two chemically similar bromine sites in $BrPPh_4$, further demonstrating how halogen NMR can detect finite changes in the crystal structure.

Experimental Section

Single-crystal X-ray diffraction: Appropriately sized single crystals of $BrPPh_4$, $BrEtPPh_3$, $BrMePPh_3$, and $Br(C_5H_9)PPh_3$ were grown in ethanol by slow evaporation, whereas one for $ClBuPPh_3$ was taken directly from the bottle sent by the manufacturer. All of the structures were solved at the X-ray Core Facility at the University of Ottawa. More detailed data collection methods, along with experimental methods for $BrPPh_4{\cdot}H_2O$, can be found in the Supporting Information.

Solid-state NMR Spectroscopy: Halogen SSNMR experiments were performed at magnetic fields of $B_0 = 9.4$ T (Bruker AVANCE III) and 11.75 T (Bruker AVANCE) at the University of Ottawa, and $B_0 = 21.1$ T (Bruker AVANCE II) at the National Ultrahigh-Field NMR Facility for Solids in Ottawa. Experimental setup and pulse calibrations were carried out with solid NH_4Cl (resonance set to $\delta = 121.1$ ppm)[48] or solid NaCl (resonance set to $\delta = 0.00$ ppm)[49] for $^{35/37}$Cl experiments, while $^{79/81}$Br experiments used solid KBr as a reference (resonance set to $\delta = 54.31$ and 54.51 ppm for ^{79}Br and ^{81}Br, respectively).[50] The CT-selective pulse or "solid-$\pi/2$", used for the phosphonium halides was that of these reference salts scaled by a factor of $1/(I+1/2) = 1/2$ as the latter pack in cubic lattices. $^{79/81}$Br SSNMR spectra were collected under stationary conditions by using the Solomon echo pulse sequence (i.e.: $\pi/2-\tau_1-\pi/2-\tau_2-acq$),[51] along with continuous-wave proton decoupling during the acquisition time.[52] Some spectra contained a broader resonance than what could be uniformly excited by the NMR probe. In those cases, it was necessary to collect multiple sub-spectra with identical acquisition parameters, but with different transmitter-frequency offsets. The co-addition of these yielded the full spectrum and is known as the variable offset cumulative spectra (VOCS) method (see Table S1 in the Supporting Information for specific details).[53,54] Spectra were also acquired under MAS conditions by using a rotor-synchronised Solomon echo pulse sequence with proton decoupling at $B_0 = 9.4$ T (for $^{35/37}$Cl experiments, $\nu_{rot} = 8$ kHz) and 21.1 T (for ^{35}Cl, $\nu_{rot} = 5$ kHz; for ^{81}Br, $\nu_{rot} = 31.25$ or 62.5 kHz (without proton decoupling)). More detailed experimental considerations (including those for ^{31}P), along with data-processing methods, can be found in the Supporting Information.

GIPAW DFT Computations: GIPAW DFT computations were performed with version 4.1 of CASTEP NMR and input files were generated by using the available crystal structure data through Materials Studio version 3.2.[30,31,32] The X-ray structures of $BrBuPPh_3$[55] and $BrHPPh_3$[56] were used as reported in the literature. On-the-fly-generated pseudopotentials were used for all atoms in the lattice and were obtained directly from Accelrys Inc. (San Diego, CA). All calculations used the Perdew, Burke, and Ernzerhof (PBE) exchange-correlation functional (XC) under the generalised gradient approximation (GGA)[57] with an ultrafine energy cut-off, E_{cut}, and k-point grid (see Table S2 in the Supporting Information). Attempts at optimising any atomic positions or unit-cell dimensions from the X-ray crystal structures was not feasible in these systems, since the unit cells were too large, even at very low E_{cut} values. Therefore, NMR calculations were performed directly on the structures generated by XRD. Phosphorus MS, as well as the bromine and chlorine EFG and MS tensors, were then extracted from the output files by using a modified version of the EFGShield program.[58] Further details on data analysis can be found in the Supporting Information.

Acknowledgements

D.L.B. thanks the Natural Sciences and Engineering Research Council (NSERC) of Canada for funding. K.M.N.B. thanks NSERC for an Alexander Graham Bell CGS M scholarship. We are grateful to Dr. Glenn Facey and Dr. Andy Lo for their technical support at the University of Ottawa NMR facilities. Dr. Victor Terskikh and Dr. Eric Ye are also acknowledged for their technical assistance and helpful training. Access to the 900 MHz NMR spectrometer was provided by the National Ultrahigh-Field NMR Facility for Solids (Ottawa, Canada), a national research facility funded by the Canada Foundation for Innovation, the Ontario Innovation Trust, Recherche Québec, the National Research Council Canada, and Bruker BioSpin and managed by the University of Ottawa (www.nmr900.ca). NSERC is acknowledged for a Major Resources Support grant.

[1] C. M. S. S. Neves, J. F. O. Granjo, M. G. Freire, A. Robertson, N. M. C. Oliveira, J. A. P. Coutinho, *Green Chem.* **2011**, *13*, 1517.
[2] C. J. Bradaric, A. Downard, C. Kennedy, A. J. Robertson, Y. Zhou, *Green Chem.* **2003**, *5*, 143.
[3] D. A. Gerritsma, A. Robertson, J. McNulty, A. Capretta, *Tetrahedron Lett.* **2004**, *45*, 7629.
[4] R. He, C. Ding, K. Maruoka, *Angew. Chem.* **2009**, *121*, 4629; *Angew. Chem. Int. Ed.* **2009**, *48*, 4559.
[5] C.-L. Zhu, F.-G. Zhang, W. Meng, J. Nie, D. Cahard, J.-A. Ma, *Angew. Chem. Int. Ed.* **2011**, *50*, 5869.
[6] J. Sun, L. Wang, S. Zhang, Z. Li, X. Zhang, W. Dai, R. Mori, *J. Mol. Catal. A Chem.* **2006**, *256*, 295.
[7] R. Cristiano, A. D. Walls, R. G. Weiss, *J. Phys. Org. Chem.* **2010**, *23*, 904.
[8] G. Wittig, U. Schöllkopf, *Chem. Ber.* **1954**, *87*, 1318.
[9] E. J. Corey, H. Yamamoto, *J. Am. Chem. Soc.* **1970**, *92*, 226.
[10] Y.-S. Hon, C.-F. Lee, *Tetrahedron* **2000**, *56*, 7893.
[11] E. L. Sukman, N. J. Montclair, (M&T Chemicals Inc. Woodbridge, N J), US patent 4.264.593, **1981**.
[12] R. Pomecko, Z. Asfari, V. Hubscher-Bruder, M. Bochenska, F. Arnaud-Neu, *Supramol. Chem.* **2007**, *19*, 459.
[13] D. Rideout, *Cancer Invest.* **1994**, *12*, 189.

[14] D. Rideout, A. Bustamante J. Patel, *Int. J. Cancer* **1994**, *57*, 247.
[15] W. A. Cooper, W. A. Bartier, D. C. Rideout, E. J. Delikatny, *Magn. Reson. Med.* **2001**, *45*, 1001.
[16] M. Doiron, J. Moulins, R. Dean, R. M. Palepu, *Phys. Chem. Liq.* **2008**, *46*, 212.
[17] P. A. Mirau, J. L. Serres, D. Jacobs, P. H. Garrett, R. A. Vaia, *J. Phys. Chem. B* **2008**, *112*, 10544.
[18] S. Bourbigot, D. L. Vanderhart, J. W. Gilman, W. H. Awad, R. D. Davis, A. B. Morgan, C. A. Wilkie, *J. Polym. Sci., Part B: Polym. Phys.* **2003**, *41*, 3188.
[19] M. Ackermann, A. Pascariu, T. Höcher, H.-U. Siehl, S. Berger, *J. Am. Chem. Soc.* **2006**, *128*, 8434.
[20] N. F. Ramsey, *Phys. Rev.* **1950**, *78*, 699.
[21] P. Pyykkö, *Mol. Phys.* **2008**, *106*, 1965.
[22] H. Trill, H. Eckert, V. I. Srdanov, *J. Am. Chem. Soc.* **2002**, *124*, 8361.
[23] H. Trill, H. Eckert, V. I. Srdanov, *J. Phys. Chem. B* **2003**, *107*, 8779.
[24] R. C. Remsing, J. L. Wildin, A. L. Rapp, G. Moyna, *J. Phys. Chem. B* **2007**, *111*, 11619.
[25] P. G. Gordon, D. H. Brouwer, J. A. Ripmeester, *J. Phys. Chem. A* **2008**, *112*, 12527.
[26] B. Alonso, D. Massiot, P. Florian, H. H. Paradies, P. Gaveau, T. Mineva, *J. Phys. Chem. B* **2009**, *113*, 11906.
[27] P. G. Gordon, D. H. Brouwer, J. A. Ripmeester, *ChemPhysChem* **2010**, *11*, 260.
[28] A. J. Rossini, R. W. Mills, G. A. Briscoe, E. L. Norton, S. J. Geier, I. Hung, S. Zheng, J. Autschbach, R. W. Schurko, *J. Am. Chem. Soc.* **2009**, *131*, 3317.
[29] J. W. E. Weiss, D. L. Bryce, *J. Phys. Chem. A* **2010**, *114*, 5119.
[30] M. D. Segall, P. J. D. Lindan, M. J. Probert, C. J. Pickard, P. J. Hasnip, S. J. Clark, M. C. Payne, *J. Phys. Condens. Matter* **2002**, *14*, 2717.
[31] C. J. Pickard, F. Mauri, *Phys. Rev. B* **2001**, *63*, 245101.
[32] M. Profeta, F. Mauri, C. J. Pickard, *J. Am. Chem. Soc.* **2003**, *125*, 541.
[33] T. Charpentier, *Solid State Nucl. Magn. Reson.* **2011**, *40*, 1.
[34] C. M. Widdifield, D. L. Bryce, *J. Phys. Chem. A* **2010**, *114*, 2102.
[35] C. M. Widdifield, D. L. Bryce, *Phys. Chem. Chem. Phys.* **2009**, *11*, 7120.
[36] E. E. Schweizer, C. J. Baldacchini, A. L. Rheingold, *Acta Crystallogr. C* **1989**, *45*, 1236.
[37] O. J. Curnow, W. T. Robinson, R. Shang, *Acta Crystallogr. E* **2007**, *63*, o3951.
[38] C. M. Widdifield, D. L. Bryce, *Can. J. Chem.* **2011**, *89*, 754.
[39] E. W. Czerwinski, *Acta Crystallogr. E* **2004**, *60*, o1442.
[40] V. P. Balema, J. W. Wiench, M. Pruski, V. K. Percharsky, *Chem. Commun.* **2002**, 724.
[41] G. Wu, V. Terskikh, *J. Phys. Chem. A* **2008**, *112*, 10359.
[42] C. M. Widdifield, D. L. Bryce, *J. Phys. Chem. A* **2010**, *114*, 10810.
[43] S. E. Ashbrook, M. Cutajar, C. J. Pickard, R. I. Walton, S. Wimperis, *Phys. Chem. Chem. Phys.* **2008**, *10*, 5754.
[44] F. Aquino, N. Govind, J. Autschbach, *J. Chem. Theory Comput.* **2011**, *7*, 3278.
[45] *Calculation of NMR and EPR Parameters: Theory and Applications* (Eds.: M. Kaupp, M. Bühl, V. G. Malkin), Wiley-VCH, Weinheim, **2004**, p. 237.
[46] R. P. Chapman, J. R. Hiscock, P. A. Gale, D. L. Bryce, *Can. J. Chem.* **2011**, *89*, 822.
[47] A. Kehrer, N. Weiden, A. Weiss, *Z. Phys. Chem. (Muenchen Ger.)* **1992**, *178*, 1.
[48] T. L. Weeding, W. S. Veeman, *J. Chem. Soc., Chem. Commun.* **1989**, 946.
[49] D. L. Bryce, G. M. Bernard, M. Gee, M. D. Lumsden, K. Eichele, R. E. Wasylishen, *Can. J. Anal. Sci. Spectrosc.* **2001**, *46*, 46.
[50] R. P. Chapman, C. M. Widdifield, D. L. Bryce, *Prog. Nucl. Magn. Reson. Spectrosc.* **2009**, *55*, 215.
[51] I. Solomon, *Phys. Rev.* **1958**, *110*, 61.
[52] A. L. Bloom, J. N. Shoolery, *Phys. Rev.* **1955**, *97*, 1261.
[53] D. Massiot, I. Farnan, N. Gautier, D. Trumeau, A. Trokiner, J. P. Coutures, *Solid State Nucl. Magn. Reson.* **1995**, *4*, 241.
[54] A. Medek, V. Frydman, L. Frydman, *J. Phys. Chem. A* **1999**, *103*, 4830.
[55] E. W. Czerwinski, *Acta Crystallogr. E* **2005**, *61*, o2272.
[56] N. Bricklebank, S. M. Godfrey, C. A. McAuliffe, R. G. Pritchard, *Acta Crystallogr. C* **1993**, *49*, 1017.
[57] a) J. P. Perdew, K. Burke, M. Ernzerhof, *Phys. Rev. Lett.* **1996**, *77*, 3865; b) J. P. Perdew, K. Burke, M. Ernzerhof, *Phys. Rev. Lett.* **1997**, *78*, 1396.
[58] S. Adiga, D. Aebi, D. L. Bryce, *Can. J. Chem.* **2007**, *85*, 496.

Received: November 4, 2011
Published online: March 20, 2012

